Effects of phase accumulation in frequency-comb-based multidimensional coherent spectroscopy

Bachana Lomsadze,* Skyler C. Weight, and Peter K. D. Hovland
Department of Physics, Santa Clara University, Santa Clara, California 95053, USA

(Received 8 April 2022; accepted 6 September 2022; published 12 September 2022)

In recent years, frequency-comb-based multidimensional coherent spectroscopy has emerged as a very powerful optical method for studying samples with long dephasing times. It enables the measurement of comb resolution multidimensional coherent spectra in seconds as opposed to hours or even days required by traditional mechanical stage-based spectrometers. However, for some samples (e.g., cold atoms and molecules) the dephasing times could be longer than the repetition periods of the excitation lasers which means that the generated signal will not fully decay between the pulses. Depending on the relative phase or time between the pulses, the signals generated by the subsequent laser pulses can constructively or destructively interfere with each other. In this paper we study this behavior by solving the optical Bloch equations and provide a theoretical description of frequency-comb-based multidimensional coherent spectroscopy.

DOI: 10.1103/PhysRevA.106.033704

I. INTRODUCTION

Since its development over two decades ago, multidimensional coherent spectroscopy (MDCS) [1,2] has attracted attention as a powerful experimental method for studying structure, nonlinear optical properties, and ultrafast dynamics of a wide range of materials [2–9]. MDCS that is based on concepts of nuclear magnetic resonance spectroscopy [10] is the only nonlinear method that can simultaneously measure homogeneous linewidth of inhomogeneously broadened systems, determine if the excited states are coupled, and also probe collective and many-body effects.

To provide more background information, in Fig. 1(a) we show a simplified schematic diagram of one of the most commonly used multidimensional coherent spectroscopy schemes. This approach is also refereed to as rephasing single quantum or photon echo [11] multidimensional coherent spectroscopy. In this approach a sequence of three pulses A* (phase conjugated pulse), B, and C (B and C are from the same pulse) are used to interrogate the sample and an emitted four-wave mixing (FWM) signal is then heterodyne detected [using local oscillator (LO) pulses] as a function of the delay between the excitation pulses (τ evolution) and the time over which it is emitted (t emission). Experimentally, the separation of the FWM and linear signals (as well as other FWM contributions) are usually performed either utilizing a "k-space" (momentum) geometry configuration [12] (FWM signal is detected in the phase matched direction $k_{\mathrm{sig}} = -k_a + k_b + k_c$) or a collinear geometry [13,14] and phase-cycling schemes (each excitation pulse is frequency tagged and the signal is detected at $f_{\mathrm{sig}} = -f_a + f_b + f_c + f_{\mathrm{LO}}$ frequency) as shown in Fig. 1(b) top and bottom. The detected time domain signal is then Fourier transformed with respect to the evolution and emission time delays to generate a multidimensional coherent spectrum.

In the photon echo excitation scheme [shown in Fig. 1(a)], the first pulse A* (a phase conjugated pulse) creates a coherence between ground ($|g\rangle$) and excited states ($|e\rangle$). This coherence then evolves with $-\omega_{ge}$ frequency. Pulse B then converts the coherence into the population state and then the same pulse converts it to the third order coherence which evolves with ω_{ge} frequency. Since the evolution (dephasing of resonances) and emission dynamics happen with the opposite phase ($-\omega_{ge}\tau$ and $\omega_{ge}t$), this enables the excited state resonances to be rephased. In the frequency domain this corresponds to separating or decoupling the samples' homogeneous and inhomogeneous linewidths [15] [see Fig. 1(c)]. In addition, this excitation scheme can distinguish a V-type system (with $\omega_1 = 2\pi f_1$ and $\omega_2 = 2\pi f_1$ resonant frequencies) from a mixture of two two-level systems with the same resonant frequencies, which is important for chemical sensing applications. This information cannot be obtained from linear absorption spectra. In Figs. 1(d) and 1(e) two-dimensional (2D) spectra are plotted for a sample containing two independent two-level systems and for a three-level V-type system, respectively. On the 2D spectra, diagonal peaks (along the white dotted line) correspond to the samples' resonances and off-diagonal peaks determine the cross peaks (evolution and emission happens at different frequencies) indicating that the resonances belong to the same system.

Rephasing single quantum 2D spectra provide critical information; however, until recently 2D spectroscopy was mostly used for samples with short dephasing times of their excited states (particularly for semiconductor materials and molecules in solutions). This is due to the fact that currently available MDCS techniques provide low spectral resolution (limited by spectrometer resolution or time delays achievable using acousto-optic modulators), or require long acquisition times (the ones implemented with long delay stages) [9]. These techniques have limitations to probe a wide range of exciting materials with long-lived excited states such as interfacial quantum dots, vacancy centers, cold atomic and molecular systems, etc. To overcome these limitations, recently, Lomsadze *et al.* have developed

*blomsadze@scu.edu

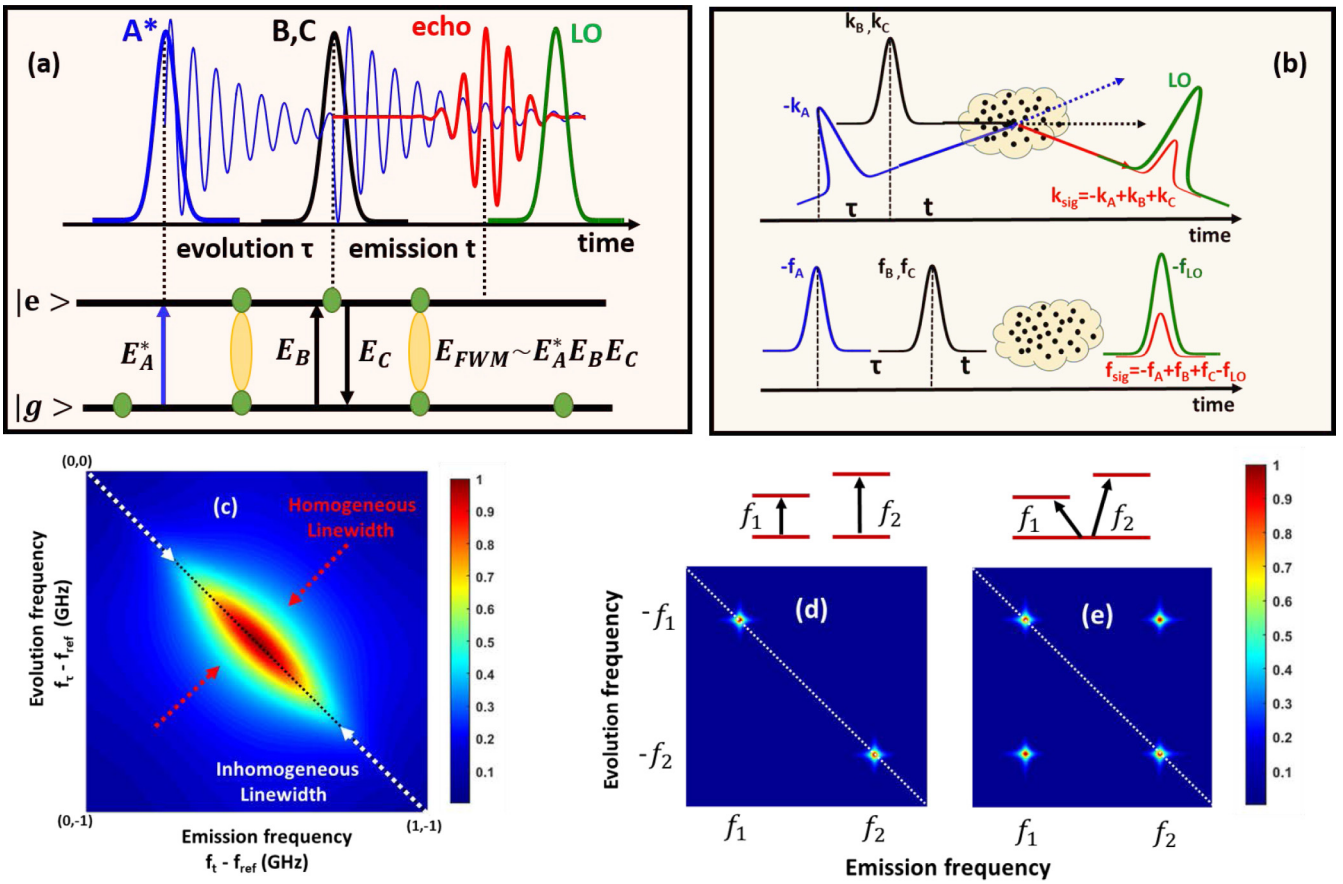

FIG. 1. (a) Photon-echo (rephasing single quantum) excitation scheme. A* (phase conjugated) pulse creates a coherence between ground ($|g\rangle$) and excited states ($|e\rangle$). This coherence then evolves during τ (blue trace). Pulse B then converts the coherence into the population state and then the same pulse (C) converts it to the third order coherence which emits a FWM signal during t (blue trace). The emitted FWM signals (from an inhomogeneously broadened system) interfere constructively at $\tau = t$ and create a photon echo signal (red). The signal is detected using an LO pulse. (b) Detection of the FWM signal using a k-space (momentum) (top) and the collinear geometry (bottom), respectively. (c) Magnitude of a photon-echo two-dimensional spectrum. The evolution frequency is negative to reflect the negative phase evolution during the evolution period. The black dotted line from (0,0) to (1, −1) GHz shows the diagonal line. White and red arrows indicate homogeneous and inhomogeneous linewidths. (d) A 2D spectrum of two independent two-level systems. g ground state, e_1 and e_2 excited states. (e) A 2D spectrum of a V-type system. Color scale shows normalized signal magnitude.

an approach to multidimensional spectroscopy that is based on the frequency-comb technology [16–19]. This approach called frequency-comb-based multidimensional coherent spectroscopy (or tri-comb spectroscopy) enables the rapid measurement of multidimensional coherent spectra with comb resolution. In this approach, the excitation and LO pulses belong to separate lasers that have slightly different repetition frequencies (e.g., $f_{\rm rep} + \Delta$, $f_{\rm rep}$, and $f_{\rm rep} - \Delta$, where $\Delta \sim$ Hz or kHz). This enables evolution and emission times (τ and t) to be scanned automatically with $\Delta/f_{\rm rep}^2$ step size up to several nanoseconds (effective time, determined by $1/f_{\rm rep}$) rapidly in seconds or milliseconds (acquisition time, determined by $1/\Delta$) without the use of mechanical delay lines [17]. Using this method it is now possible to investigate critical processes in cold atomic or molecular samples and vacancy centers that are promising candidates for quantum computing.

However, it is important to note that the excited states' dephasing times for some of the samples mentioned above are usually much longer than the repetition periods of the lasers used in frequency-comb-based multidimensional coherent spectroscopy. For example, dephasing times for alkali metal atoms in a magneto-optical trap (MOT) are tens to hundreds of nanoseconds [20], whereas repetition periods of frequency combs are typically a few nanoseconds. In this situation a FWM signal generated in the sample is not decayed between the comb pulses and hence will interfere with the FWM signal generated by the next sequence of the comb pulses. This process is pictorially shown in Fig. 2(a). Depending on the samples' resonance frequencies, dephasing times, and relative phase between the comb pulses (determined by the repetition period and the carrier envelope phase) these FWM signals can constructively or destructively interfere with each other. By controlling the relative phase between the pulses, one can control the strength of FWM signals and hence the peaks on a 2D spectrum.

The goal of this paper is to provide a theoretical description of frequency-comb-based multidimensional coherent

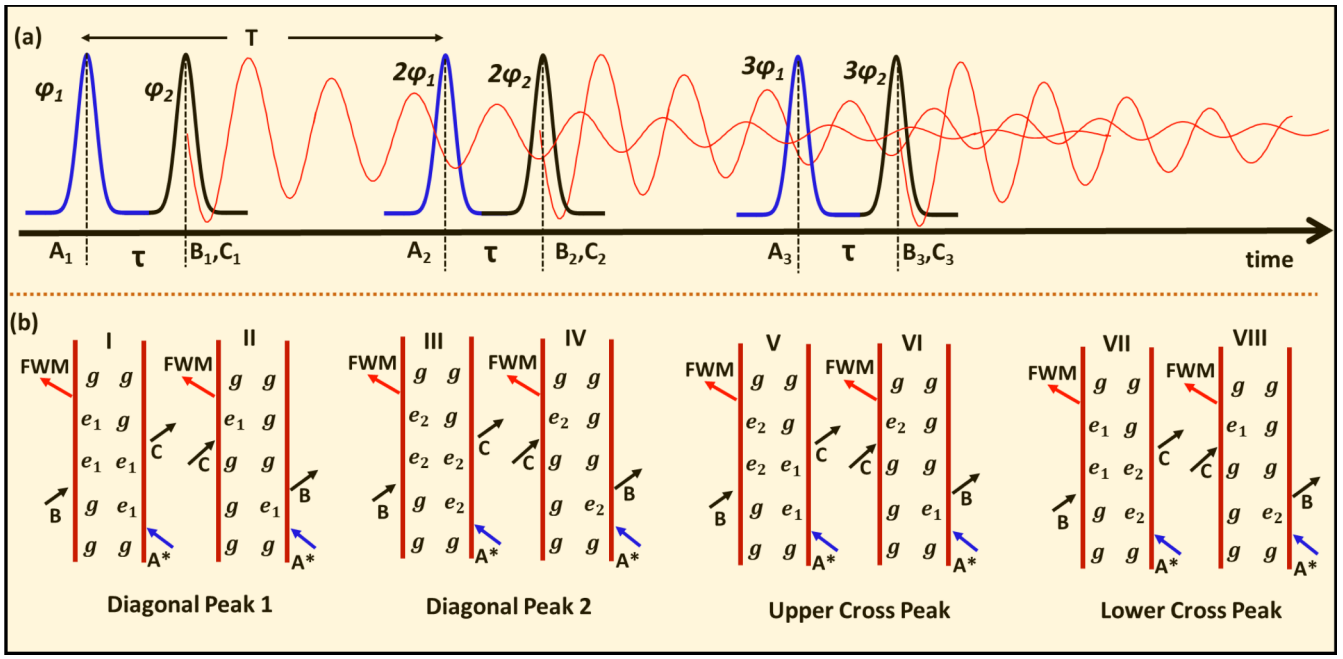

FIG. 2. (a) Photon-echo (rephasing single quantum) excitation scheme using two trains (blue and black) of pulses. T repetition period of each train. and φ_1 and φ_2 correspond to carrier envelope phase slips for each train. Red curves show the four-wave mixing signals. FWM signal generated by A^*_1, B_1, C_1 interferes with the signals generated by A^*_2, B_2, C_2 and A^*_3, B_3, C_3. (b) Feynman diagrams contributing to the generation of the photon echo FWM signal. I and II correspond to diagonal peak 1 (upper left corner) in Fig. 1(e), III and IV correspond to diagonal peak 2 (lower right corner), V and VI correspond to the lower cross peak (lower left corner), and VII and VIII correspond to the upper cross peak (upper right corner).

spectroscopy of samples whose dephasing times are longer than the repetition periods of the excitation lasers. We hope that the results will provide valuable insights into comb-based MDCS and will help efforts to extend MDCS to cold atomic and molecular systems.

II. SIMULATION AND RESULTS

To demonstrate the effects of phase accumulation in frequency-comb-based multidimensional coherent spectroscopy, we solved the optical Bloch equations for a three-level V system shown in Fig. 1(e),

$$\dot{\rho} = -\frac{i}{\hbar}[H_0, \rho] - \frac{i}{\hbar}[H_{\text{int}}, \rho] - \gamma\rho. \tag{1}$$

In this equation ρ is the density matrix, γ describes the decay rates of the excited states and coherences, $H_0 = \hbar\omega_1 |e_1\rangle\langle e_1| + \hbar\omega_2 |e_2\rangle\langle e_2|$ is the unperturbed Hamiltonian describing the three-level V system with ω_1 and ω_2 resonant frequencies, $H_{\text{int}} = \mu_{ge_1}E(t)|g\rangle\langle e_1| + \mu_{ge_2}E(t)|g\rangle\langle e_2| + \text{H.c.}$ is the perturbation due to the laser electric fields $E(t)$, and μ_{ge_1} and μ_{ge_2} are the transition dipole strength of the excited states. In our simulation the system is subjected to two trains [Fig. 2(a)] of equally spaced ultrashort pulses (Delta-function pulses $E(t) \approx E_0 e^{i\omega t}\delta(t - nT)e^{in\varphi}$, where T is the repetition period of the laser, φ is the carrier envelope phase (CEP) slip, and n is an integer). Each train contains equally spaced identical pulses, except that each pulse (in each train) is differed from the previous one by a carrier-envelope phase (CEP) slip (φ_1 and φ_2, which are controlled parameters in our calculation) [21]. In order to resemble a real system and also decrease the computation time, we chose the repetition periods of our lasers to be $T = 2$ ns ($f_{\text{rep}} = 500$ MHz), and the sample's natural decoherence time to be 20 ns ($\gamma = 50$ MHz). This is equivalent to probing a sample whose pure decoherence time is ∼100 ns (e.g., alkali metal atoms in a magneto-optical trap) using ∼10 ns (most commonly used) repetition period frequency combs. In our simulation we treated our system to be homogeneously broadened (e.g., atoms in a MOT) and followed the Feynman diagrams [shown in Fig. 2(b)] to isolate the contributions of signals related to the photon-echo excitation scheme. In this scheme, the third order polarization [$P = \text{Tr}(\mu\rho)$] induced by a pair of comb pulses [e.g., A^*_n, B_n, and C_n in Fig. 2(a)] is

$$\begin{aligned} P(t,\tau) = {} & 2(-i/\hbar)^3 E_0^3 \mu_{ge_1}^4 \exp[-i\omega_1\tau + i\omega_1 t - \gamma_1(t+\tau) + in(2\varphi_2 - \varphi_1)] \\ & + 2(-i/\hbar)^3 E_0^3 \mu_{ge_2}^4 \exp[-i\omega_2\tau + i\omega_2 t - \gamma_2(t+\tau) + in(2\varphi_2 - \varphi_1)] \\ & + 2(-i/\hbar)^3 E_0^3 \mu_{ge_1}^2 \mu_{ge_2}^2 \exp[-i\omega_1\tau + i\omega_2 t - (\gamma_2 t + \gamma_1\tau) + in(2\varphi_2 - \varphi_1)] \\ & + 2(-i/\hbar)^3 E_0^3 \mu_{ge_1}^2 \mu_{ge_2}^2 \exp[-i\omega_2\tau + i\omega_1 t - (\gamma_1 t + \gamma_2\tau) + in(2\varphi_2 - \varphi_1)]. \end{aligned} \tag{2}$$

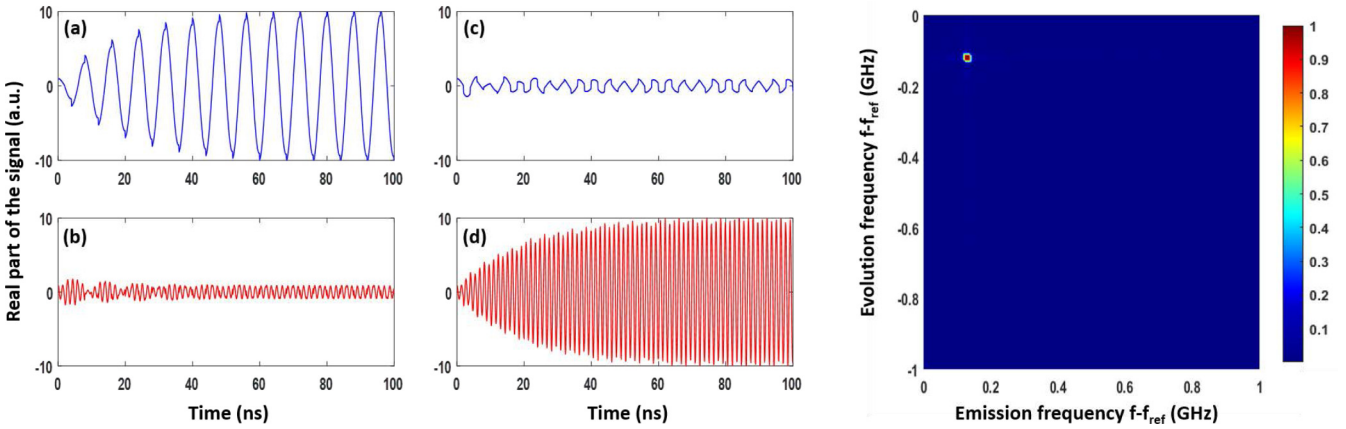

FIG. 3. (a) and (b) Normalized strength of the real parts of the one-dimensional (1D) FWM signals emitted at $\omega_1 = 125 \cdot 2\pi$ MHz and $\omega_2 = 725 \cdot 2\pi$ MHz frequencies, respectively. The results were obtained for $\tau = 0$, $\varphi_1 = \varphi_2 = 0.5\pi$, and $\gamma_1 = \gamma_2 = 50$ MHz. (c) and (d) Normalized strength of the real parts of the 1D FWM signals emitted at $\omega_1 = 125 \cdot 2\pi$ MHz and $\omega_2 = 725 \cdot 2\pi$ MHz frequencies, respectively. The results were obtained for $\tau = 0$, $\varphi_1 = \varphi_2 = 0.9\pi$, and $\gamma_1 = \gamma_2 = 50$ MHz. (e) Magnitude of a 2D spectrum for a V-type system with $\omega_1 = 125 \cdot 2\pi$ MHz and $\omega_2 = 725 \cdot 2\pi$ MHz resonant frequencies. $\varphi_1 = \varphi_2 = 0.5\pi$. $f_{\text{ref}} = 300$ THz arbitrary optical reference. Color scale shows normalized signal magnitude.

In the equation E_0 is the magnitude of the excitation pulses (assumed identical), $\mu_{ge_1} = \mu_{ge_2}$ and $\gamma_1 = \gamma_2$ are the transition dipole strength and decoherence rates for $|e_1\rangle$ and $|e_2\rangle$ excited states, respectively. $\omega_1 = \omega_{ge_1} - \omega_{\text{ref}}$ and $\omega_2 = \omega_{ge_2} - \omega_{\text{ref}}$, where ω_{ge_1} and ω_{ge_2} are resonant frequencies for $|e_1\rangle$ and $|e_2\rangle$ excited states and $\omega_{\text{ref}} = 300 \cdot 2\pi$ THz is an arbitrary reference frequency. φ_1 and φ_2 are the carrier envelope phase slips for comb A and comb B (C) and n is an integer (that varies from 0 to 50 (number of pulses in the train)). The first term in the equation corresponds to the absorption and emission at ω_1 frequency [I and II Feynman diagrams in Fig. 2(b)], the second term corresponds to the absorption and emission at ω_2 frequency [III and IV Feynman diagrams in Fig. 2(b)], whereas the third and forth term correspond to the absorption and emission at ω_1 (ω_2) and ω_2 (ω_1) frequencies [V and VI (VII and VIII) Feynman diagrams in Fig. 2(b)]. To include the effects of multiple pulses, first we fixed τ delay, calculated the FWM signals for each pair of comb pulses (total of 50), and then we added them coherently in the regions where they overlapped. The results for $\tau = 0$, $\varphi_1 = \varphi_2 = 0.5\pi$, $\omega_1 = 125 \cdot 2\pi$ MHz, $\omega_2 = 725 \cdot 2\pi$ MHz, and $\gamma_1 = \gamma_2 = 50$ MHz are shown in Figs. 3(a) and 3(b). The effects of the phase accumulation is obvious. For the values listed above, the FWM signals emitted at ω_1 are constructively interfering (hence it is growing), whereas they destructively interfere at ω_2 emission frequency. One can reverse the picture by adjusting either the repetition period or carrier envelope phase slip of each pulse train [21]. Experimentally this can be done by adjusting one of the laser mirrors in the cavity or the pump power. The results for $\varphi_1 = \varphi_2 = 0.9\pi$ are plotted in Figs. 3(c) and 3(d) which clearly shows that now the FWM signals emitted at ω_2 are constructively interfering, whereas they destructively interfere at ω_1 emission frequency.

To generate a two-dimensional spectrum, we then varied τ from 0 to 50 T (T-repetition period = 2 ns) and calculated FWM signals for each delay. The delay beyond 2 ns is equivalent to including contributions from the FWM signals generated by, e.g., A^*_1, B_2, C_2; A^*_2, B_3, C_3; A^*_1, B_3, C_3; etc. The total FWM signal was then Fourier transformed with respect to τ and t. The resulting 2D spectrum for $\varphi_1 = \varphi_2 = 0.5\pi$ is shown in Fig. 3(e). On this 2D spectrum it is clear that, due to constructive or destructive interference along τ and t times, only the peak at $(-f_1, f_1)$ is dominant and other diagonal $(-f_2, f_2)$ and cross peaks $[(-f_1, f_2)$ and $(-f_2, f_1)]$ are not even visible. We should also note that the peak on the spectrum corresponds to a single point of the excited state's line shape and does not reflect the full profile (both diagonal and cross diagonal) of the excited state's resonance. In order to obtain the full line shape as well as observe other diagonal and cross peaks, one needs to adjust either the repetition period or CEP slips of the excitation combs, acquire multiple 2D spectra (one for each phase), and combine them into a single 2D spectrum. While doing so it is important to know that the constructive or destructive interference of FWM signals along the evolution time is determined by $\varphi_\tau = -\varphi_1$ phase slip and along the emission time is determined by $\varphi_t = -\varphi_1 + 2\varphi_2$ phase slip. If the full profile of a 2D spectrum is desired, then one can scan φ_τ and φ_t iteratively. The results are shown in Fig. 4(a). It is also possible to obtain a specific peak instead of acquiring the full 2D spectrum. For example, in Figs. 4(b) and 4(c), by choosing specific φ_τ and φ_t values, only upper diagonal and lower cross peaks were acquired, respectively. One can also acquire the diagonal profile of a specific peak by anticorrelating the φ_τ and φ_t values [scanning them simultaneously in the opposite direction $(\varphi_t = \varphi_o - \varphi_\tau)$] and one can obtain the cross diagonal profile by correlating the φ_τ and φ_t values ($\varphi_t = \varphi_o + \varphi_\tau$, scanning them in the same direction). In these expressions the value of φ_o (offset phase) determines the section (diagonal or off-diagonal) that is scanned on a 2D spectrum. The diagonal and cross-diagonal profiles of the lower diagonal ($\varphi_o = 0$) and upper cross peaks ($\varphi_o = 1.4\pi$) are shown in Figs. 4(d) and 4(e), respectively.

A simple explanation of how one can target a specific peak on a 2D spectrum is as follows: the diagonal and cross peaks correspond to absorption and emission at different frequencies and hence one can "tune" the phases of both frequency combs

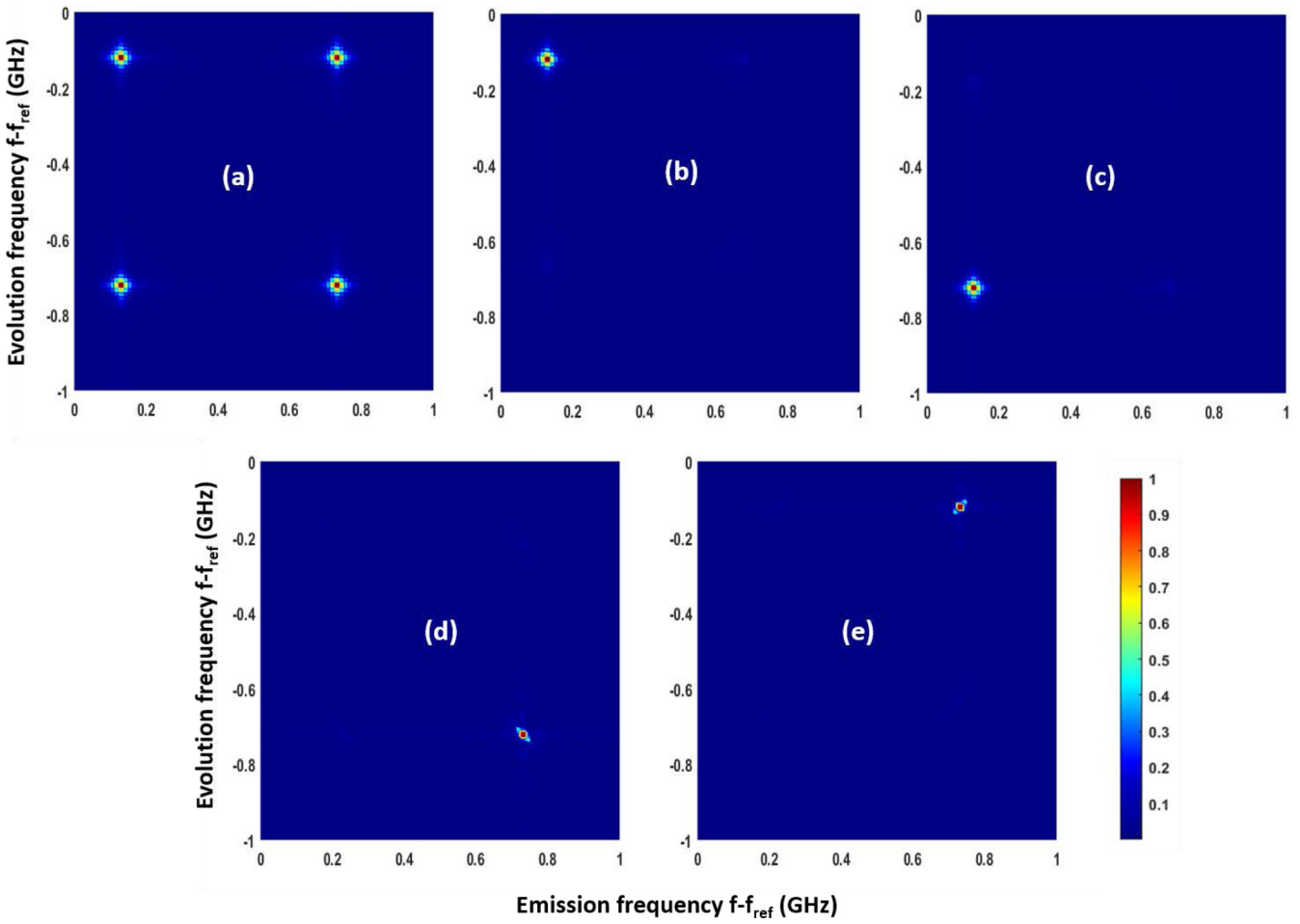

FIG. 4. Magnitude of overlaid 2D spectra for a V-type system with $\omega_1 = 125 \cdot 2\pi$ MHz and $\omega_2 = 725 \cdot 2\pi$ MHz resonant frequencies. (a) The spectrum was acquired by scanning φ_1 and φ_t values iteratively from 0.3π to 1.1π with 0.05π step size, respectively. (b) The spectrum was acquired by scanning φ_1 and φ_t values iteratively from 0.3π to 0.7π with 0.05π step size, respectively. (c) The spectrum was acquired by scanning φ_1 and φ_t values iteratively from 0.7π to 1.1π and from 0.3π to 0.7π with 0.05π step size, respectively. (d) The spectrum was acquired by scanning φ_1 and φ_t values simultaneously from 0.7π to 1.1π. (e) The spectrum was acquired by scanning φ_1 (from 0.3π to 0.7π) and φ_t (from 1.1π to 0.7π) simultaneously. $f_{\text{ref}} = 300$ THz arbitrary optical reference. Color scale shows normalized signal magnitude.

such that the FWM signals, corresponding to a specific peak, constructively interfere both along t and τ times simultaneously. If the frequency separation between the excited states is not exactly equal to an integer number times the repetition frequency of the excitation lasers (which is the case for most samples), then the "tuning" for each peak happens at different sets of φ_1 and φ_2 values (φ_τ and φ_t). One can think about this process as using a very high resolution, extremely narrow, and tunable bandpass filters along the evolution and emission frequencies. This is a useful capability as it allows one to monitor a specific peak on a congested spectrum as a function of other experimental parameters, or even measure a specific 2D profile. Clearly this cannot be accomplished using regular optical bandpass filters and traditional MDCS experimental setups.

We note that the calculation shown above describes only a photon-echo excitation scheme (A*, B, C), however since the samples' dephasing time is longer than the repetition periods of the excitation lasers, the detected FWM signal will contain contributions from the (B, C, A*) excitation scheme as well. A 2D spectrum obtained in this scheme is refereed to as a double-quantum spectrum and provides insight of many-body effects and interactions. To understand this point, below, first we provide a brief overview of how 2D spectroscopy is used to probe many-body effects [8,22,23] and then we show the results of our calculation in the (B, C, A*) excitation scheme.

III. PROBING MANY-BODY EFFECTS

Double-quantum coherent spectroscopy [8,18,22,23] is similar to single-quantum coherent spectroscopy except that the time ordering of the excitation pulses are swapped (B, C, A*) [Fig. 5(a)]. In this excitation scheme the first pulse (B) excites a coherence between the ground and singly excited states and then the same pulse (C) excites the coherence between the ground state and the doubly excited state (also referred to as a double-quantum coherence). This coherence evolves with ω_{fe} frequency. The phase conjugated pulse (A*) then puts the system either back into the coherence between the ground and the singly excited states or into the coherence between the singly excited and doubly excited states. The final radiated signal is then detected and Fourier transformed

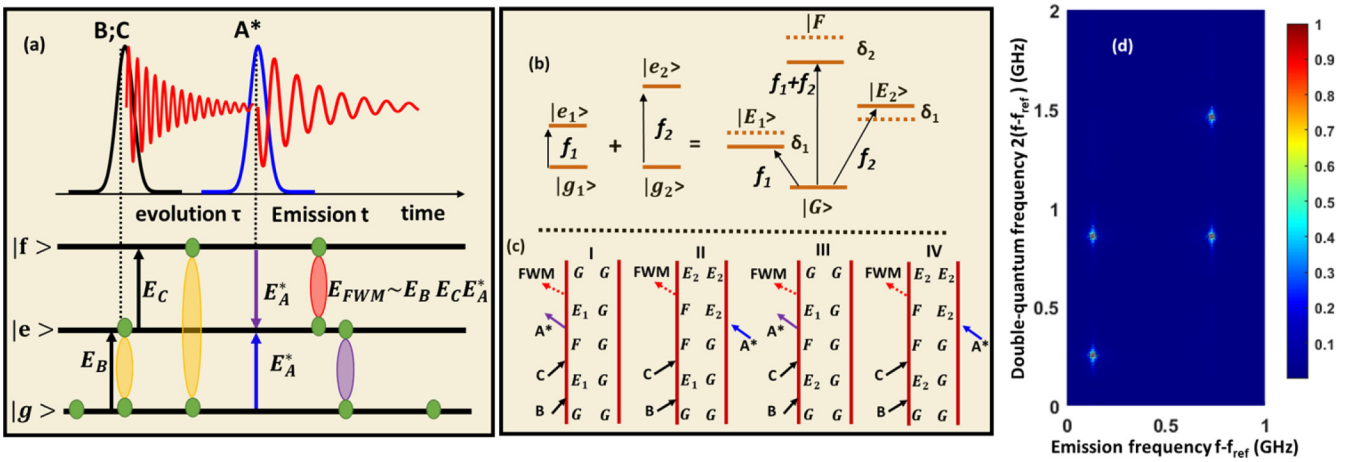

FIG. 5. (a) Double-quantum excitation scheme: $|g\rangle$ ground state, $|e\rangle$ excited state, $|f\rangle$ doubly excited state. (b) Combined picture of two two-level systems (with f_1 and f_2 resonance frequencies) without interaction (solid lines) and with interactions (dotted lines). $|G\rangle$ both atoms are on the ground state, $|E_1\rangle$ and $|E_1\rangle$ either atom 1 or atom 2 is excited, $|F\rangle$ both atoms are excited. δ_1 and δ_2 correspond to frequency shifts of $|E_1\rangle$ ($|E_2\rangle$) and $|F\rangle$ states, respectively. (c) Double-sided Feynman diagrams of the FWM signals corresponding to $f_1 + f_2$ evolution and f_1 emission frequencies in a double-quantum excitation scheme (B,C,A*). (d) Magnitude of overlaid double-quantum 2D spectra for a V-type system with $\omega_1 = 125 \cdot 2\pi$ MHz and $\omega_2 = 725 \cdot 2\pi$ MHz resonant frequencies. The spectrum was acquired by scanning φ_2 and φ_t values iteratively from 0.3π to 1.1π, respectively. Color scale shows normalized signal magnitude.

with respect to τ and t to generate a 2D spectrum. Clearly double-quantum MDCS can measure doubly excited states, however, it can also probe samples that do not have double excited states (or they are outside the bandwidth of the laser pulses), e.g., two-level systems shown in Fig. 1(d). In that case the generation of a FWM signal can be described by combining (performing Hilbert space transformation) simple two two-level systems as shown in Fig. 5(b) (solid lines) which clearly shows a doubly excited state. In this combined picture, $|G\rangle$ corresponds to both atoms being on the ground state, $|E_1\rangle$ and $|E_2\rangle$ correspond to atom 1 or atom 2 being on the excited state, and $|F\rangle$ corresponds to both atoms being on the excited states. In this excitation scheme, the pathways that could potentially lead to the generation of FWM signals (for example the ones corresponding to $f_1 + f_2$ evolution and f_1 emission frequencies) are described using the double-sided Feynman diagrams [Fig. 5(c)]. However, following the double-sided Feynman diagram rules, the contributions completely cancel each other as all FWM signals have exactly the same emission frequency, the same strength, and opposite sign (I and III are negative, II and IV are positive). This is not surprising as the signal generation should not depend on the basis used to describe the process. If there is no signal in the two independent atoms basis, there will be no signal in the combined picture as well.

The result is true if there is no interaction between the atoms, however, if we include dipole-dipole interactions, then each state will experience a slight energy shift as shown in Fig. 5(b) with dotted lines (or slight changes in decoherence rates). In this case the FWM signal contributions emitted by the sample do not perfectly cancel each other and hence leads to a nonzero signal. To demonstrate this point, in our calculation (optical Bloch equations) we included slight energy level shifts δ_1 and δ_2 (~kHz) due to dipole-dipole interactions and followed the Feynman diagrams shown in Fig. 5(c) to isolate the contributions of signals related to the double-quantum excitation scheme. In this scheme the third order polarization induced by a pair of comb pulses in the $|ge_1\rangle$ and $|ge_2\rangle$ interacting system [shown in Fig. 5(b)] is

$$P_{\mathrm{DQ}}(t,\tau) = 2(-i/\hbar)^3 E_0^3 \mu_{ge_1}^2 \mu_{ge_2}^2 \{\exp[i(\omega_1+\omega_2+\delta_2)\tau + i(\omega_1+\delta_1+\delta_2)t - \gamma t - 2\gamma\tau + in(2\varphi_2-\varphi_1)] - \exp[i(\omega_1+\omega_2+\delta_2)\tau + i(\omega_1+\delta_1)t - \gamma t - 2\gamma\tau + in(2\varphi_2-\varphi_1)]\}. \quad (3)$$

For a three-level V-type system, considered in this work, there are dipole-dipole interactions between $|ge_1\rangle$ and $|ge_1\rangle$ states, $|ge_2\rangle$ and $|ge_2\rangle$ states, and $|ge_2\rangle$ and $|ge_1\rangle$ states as well that produce similar third order polarization terms. All of these third order polarization terms were included in our calculation and the final signal (including the contributions from different excitation pulses) was then Fourier transformed with respect to τ and t. The result is plotted in Fig. 5(d) which was acquired by scanning φ_2 and φ_t values iteratively from 0.3π to 1.1π. The peaks along the diagonal (from [0, 0] to [1, 2] GHz) correspond to coupling between the same $|e_1\rangle$ and $|e_2\rangle$ energy levels of two V-type systems (atoms), respectively, and cross-diagonal peaks correspond to coupling between $|e_1\rangle$ and $|e_2\rangle$ energy levels of two atoms. These peaks are only due to dipole-dipole interactions.

The description shows that, the combination of single-quantum [Fig. 4(a)] and double-quantum [Fig. 5(d)] spectra provide critical and complete spectroscopic information and in frequency-comb-based MDCS they can be obtained simultaneously, even though the emitted FWM signals are overlapped. Furthermore, if necessary, by controlling the CEP slips of combs A and B, one can obtain high resolution sections of single-quantum and double-quantum 2D spectra.

Before we conclude, we note that in recent years there has been substantial progress in developing high repetition rate (tens to hundreds of GHz) frequency combs (e.g., microcombs) [24]. These lasers clearly are suitable for probing samples with short dephasing times (e.g., semiconductor materials and molecules in solutions) and hence the analysis described in this paper can readily be extended to the systems as well.

IV. CONCLUSION

In this work we provided a theoretically description of frequency-comb-based multidimensional coherent spectroscopy of systems whose dephasing times are longer than the repetition periods of the excitation lasers. We showed that single-quantum and double-quantum 2D spectra are obtained simultaneously and the strength of diagonal and off-diagonal peaks contain contributions from the FWM signals generated by different pairs of excitation pulses. By varying the relative phase between the excitation pulses, one can precisely control which contributions interfere constructively or destructively and hence resolve and display or target specific peaks on a 2D spectrum with high resolution. These improvements now make MDCS relevant for systems with narrow resonances, e.g., cold atomic and molecular (homonuclear and heteronuclear) samples that have very narrow fine or hyperfine and rovibrational lines. Until now, these measurements were challenging with currently available MDCS methods due to their resolution limitations and long acquisition times. In addition, frequency-comb-based MDCS will enable us to probe these systems in a MOT (e.g., rubidium) and Bose-Einstein condensate to study many-body interactions and collective effects, determine the interaction range and number of atoms that contribute in the collective response, and determine energy transfer dynamics between the excited states with fs resolution. Furthermore, the method can also be used to map out potential energy curves and probe optical properties of ultra-long-range Rydberg molecules, also known as trilobite molecules [25]. These exotic molecules have very unique properties. They are the most polar molecules ever created, even though they are homonuclear. They have very high binding energies (∼GHz), and have extremely long radiative lifetimes (∼tens to hundreds of μs). These are the properties that make them very attractive for possible applications in quantum information and frequency-comb-based MDCS is a powerful technique to study these materials with high resolution. We hope that the theoretical description and results shown in this paper provide valuable insights into comb-based 2D spectroscopy and will aid efforts to extend MDCS to cold atomic and molecular systems.

ACKNOWLEDGMENT

The research is based on work supported by the National Science Foundation (NSF) (Grant No. 1904704).

[1] S. Cundiff and S. Mukamel, Phys. Today **66**(7), 44 (2013).
[2] P. Hamm and M. Zanni, *Concepts and Methods of 2D Infrared Spectroscopy* (Cambridge University Press, Cambridge, 2011).
[3] M. Thämer, L. De Marco, K. Ramasesha, A. Mandal, and A. Tokmakoff, Science **350**, 78 (2015).
[4] C. L. Smallwood and S. T. Cundiff, Laser Photonics Rev. **12**, 1870052 (2018).
[5] V. Tiwari, Y. A. Matutes, A. Konar, Z. Yu, M. Ptaszek, D. F. Bocian, D. Holten, C. Kirmaier, and J. P. Ogilvie, Opt. Express **26**, 22327 (2018).
[6] B. Lomsadze and S. T. Cundiff, IEEE Photonics Technol. Lett. **31**, 1886 (2019).
[7] V. Tiwari, J. Chem. Phys. **154**, 230901 (2021).
[8] D. Liang and H. Li, J. Chem. Phys. **154**, 214301 (2021).
[9] M. Cho, *Coherent Multidimensional Spectroscopy* (Springer, Berlin, 2019), Vol. 226.
[10] R. R. Ernst, G. Bodenhausen, and A. Wokaun, *Principles of Nuclear Magnetic Resonance in One and Two Dimensions* (Oxford University Press, Oxford, 1987).
[11] N. A. Kurnit, I. D. Abella, and S. Hartmann, Phys. Rev. Lett. **13**, 567 (1964).
[12] A. D. Bristow, D. Karaiskaj, X. Dai, T. Zhang, C. Carlsson, K. R. Hagen, R. Jimenez, and S. T. Cundiff, Rev. Sci. Instrum. **80**, 073108 (2009).
[13] P. F. Tekavec, G. A. Lott, and A. H. Marcus, J. Chem. Phys. **127**, 214307 (2007).
[14] B. Lomsadze and S. T. Cundiff, Opt. Lett. **42**, 2346 (2017).
[15] M. E. Siemens, G. Moody, H. Li, A. D. Bristow, and S. T. Cundiff, Opt. Express **18**, 17699 (2010).
[16] B. Lomsadze and S. T. Cundiff, Science **357**, 1389 (2017).
[17] B. Lomsadze, B. C. Smith, and S. T. Cundiff, Nat. Photonics **12**, 676 (2018).
[18] B. Lomsadze and S. T. Cundiff, Phys. Rev. Lett. **120**, 233401 (2018).
[19] B. Lomsadze and S. T. Cundiff, Sci. Rep. **7**, 14018 (2017).
[20] A. Marian, M. C. Stowe, J. R. Lawall, D. Felinto, and J. Ye, Science **306**, 2063 (2004).
[21] J. Ye and S. T. Cundiff, *Femtosecond Optical Frequency Comb: Principle, Operation and Applications* (Springer Science & Business Media, New York, 2005).
[22] F. Gao, S. T. Cundiff, and H. Li, Opt. Lett. **41**, 2954 (2016).
[23] X. Dai, M. Richter, H. Li, A. D. Bristow, C. Falvo, S. Mukamel, and S. T. Cundiff, Phys. Rev. Lett. **108**, 193201 (2012).
[24] T. J. Kippenberg, R. Holzwarth, and S. A. Diddams, Science **332**, 555 (2011).
[25] D. Booth, S. T. Rittenhouse, J. Yang, H. R. Sadeghpour, and J. P. Shaffer, Science **348**, 99 (2015).